Residual stability of sessile droplets with negative line tension

Luca Guzzardi*
Dipartimento di Matematica, Università di Firenze, Viale Morgagni 67a, 50134 Firenze, Italy and Dipartimento di Matematica, Università di Pavia, Via Ferrata 1, 27100 Pavia, Italy

Riccardo Rosso† and Epifanio G. Virga‡
Dipartimento di Matematica and CNISM, Università di Pavia, Via Ferrata 1, 27100 Pavia, Italy
(Received 26 July 2005; revised manuscript received 11 October 2005; published 6 February 2006)

We study the local stability of a sessile droplet with nonvanishing line tension along the contact line, where three phases are in equilibrium. We confirm Widom's results [J. Phys. Chem. **99**, 2803 (1995)] on the local stability of a droplet with positive line tension in a larger class of perturbations. When the line tension is negative, we prove that the restricted class of perturbations employed by Widom fails to capture the instability of equilibria. A notion of residual stability is introduced, which makes quantitative the condition under which equilibrium of droplets with negative line tension are likely to be observed.

DOI: 10.1103/PhysRevE.73.021602 PACS number(s): 68.08.Bc

I. INTRODUCTION

The stability of sessile droplets is a major topic in wetting science. Although this is a topic with a long history, in the past few years it has received renewed attention because new challenges have been posed by the availability of experimental techniques able to explore reliably length scales in the micrometer range and by the urge of technological applications in nanofluids. Section 2 of [1] reviews applications that directly involve line-tension effects. As a consequence, the classical problem of finding the equilibrium of a sessile droplet on a flat, homogeneous substrate has been revived, and a plethora of new phenomena, challenging both physicists and mathematicians, has been revealed.

We are mostly concerned with the effects of line tension on the equilibrium and stability of droplets. Line tension was originally introduced by Gibbs in his seminal paper [2] by analogy with surface tension. In fact, as surface tension measures the excess free energy along an interface separating two distinct phases, line tension measures the excess free energy along a contact line where three distinct phases coexist in equilibrium. In [2], Gibbs also heeded an important difference between surface and line tensions: while the former must be positive, the latter can have either sign.

Accounting for line tension affects the equilibrium of droplets, since Young's equation, which governs the shape of the contact line, is altered. The generalized Young's equation establishes a relation between line tension and the droplet's contact angle, which also involves the geometric properties of the contact line. Line-tension measurements are based upon this equation and for several reasons—above all, the small length scales at which the effects of line tension are perceptible—they provided values of either sign also differing from one another by several orders of magnitude.

The main theoretical objection against a negative line tension is that the free-energy functional—whose minima should represent stable, and hence observable, equilibria—is unbounded from below, so that every equilibrium configuration can be made unstable by suitably selecting a perturbing mode [3,4]. The crucial point, however, is to determine the typical length associated with destabilizing modes. If this length is shorter than a typical microscopic length ℓ_{mic}, the instability is simply inconsistent with the continuum model that describes the droplet's equilibria. The microscopic length ℓ_{mic} can be identified with the intrinsic width of the contact line [5]; experimental estimates for it range from 1 to 100 times the molecular length ℓ_{mol} [6]. Below, whenever we need a specific estimate for ℓ_{mic}, we shall use the average value $\ell_{\mathrm{mic}} \approx 50 \ell_{\mathrm{mol}}$.

More specifically, even the hypothesis of constant surface tension is tenable only if the size of the droplet is much larger than the range of intermolecular forces [7], and indeed curvature corrections have been considered for surface tension [8]. Similar corrections were introduced long ago for line tension too [9], but this formal theory has too many parameters to be tractable. Here all these corrections are ignored.

This paper has a different objective; it builds upon a stability criterion worked out in [10] and applied in [11] to explore the stability of liquid bridges in the presence of line-tension. This criterion is general enough to cover line-tension effects as well as inhomogeneities and arbitrary shapes of the substrate. A similar criterion was later introduced in [12] and recently applied to the stability of liquid bridges (also called liquid filaments), where it led to conclusions consistent with ours [6]. Sekimoto, Oguma, and Kawasaki [13] had also performed a stability analysis. While they covered several wetting morphologies, by considering even doughnut droplets, their analysis was restricted to homogeneous, flat substrates and, more importantly, it was confined to small contact angles, while no similar restriction is imposed in [10].

We consider a sessile droplet lying on a homogeneous, rigid, flat substrate, in the presence of line tension. This problem has been already studied by Widom in [7]. He com-

*Electronic address: loki_delgado@hotmail.com
†Electronic address: riccardo.rosso@unipv.it
‡Electronic address: virga@imati.cnr.it

pared the free energy of a sessile droplet with nonzero line tension and that of a spherical droplet with the same volume. He found a first-order drying transition occurring when the line tension exceeds a positive critical value. For negative line tensions, the sessile droplet was found to be locally stable with respect to perturbations that preserve the spherical shape of its free surface. For positive line tensions, Widom found two equilibria, of which only one is metastable, provided that the line tension does not exceed a threshold, beyond which no equilibrium configuration exists. These conclusions were arrived at within the rather specific class of perturbations that map spheres into spheres. Strictly speaking, these results can only be interpreted as necessary conditions for stability.

It is the aim of this paper to examine to which extent the class chosen by Widom captures the stability of sessile droplets laid on a flat substrate. We employ a local stability criterion, suitable to detect metastability limits, which allows perturbations far more general than Widom's. As a result, while we confirm Widom's metastability limits when the line tension is positive, we detect unstable modes when the line tension is negative.

For every negative value of the line tension, there are destabilizing modes that make the droplet's contact line increasingly corrugated. This statement, plain as it may appear, calls for a careful interpretation. Whenever use is made of a continuum model, all length scales it involves should be larger than the typical microscopic length ℓ_{mic}, at which scale a continuum approach would be unrealistic. The perturbing modes should also be treated accordingly [6]. Modes with a characteristic wavelength smaller than ℓ_{mic} will here be discarded, as they induce perturbations existing outside the realm of validity of a continuum approach. To ensure compatibility to the continuum model employed here, both length scales it conceals—that is, the typical size R of a droplet and the ratio $|\xi|$ between the magnitudes of line and surface tensions—must be larger than ℓ_{mic}. Assessing the smallest wavelength ℓ_m of a perturbing mode of the droplet turns out to be slightly more involved than one would intuitively anticipate. We found it convenient arriving at ℓ_m through the notion of *residual* stability and an associated integer index that measures its degree. Any equilibrium configuration of the droplet is said to be residually stable if there is at least one stable mode. The highest index of all stable modes is the index of residual stability. An equilibrium configuration is stable only if all modes are stable. The main outcome of our study is to show that a droplet is residually stable provided that the line tension, when negative, is small in magnitude. Residual stability has the potential to explain experimental observations reporting negative line tensions.

This paper is organized as follows. Section II is devoted to the generalized Young equation: for positive line tension, either two or no equilibria exist; for negative line tension, only one equilibrium exists. Section III concerns the stability of these equilibria. After a technical premise, where the stability criterion we employ is recalled and applied to the problem at hand, we organize our results into two distinct subsections: one for each sign of line tension. We compute the index of residual stability for a set of experimental data indicating the observation of negative line tensions [14]. Finally, a closing section summarizes the contents of the paper and indicates the prospects for future work. To ease the presentation, the mathematical details of the modal analysis are explained in seven short appendixes.

II. EQUILIBRIA

Here we find the equilibrium configurations of a droplet $\mathcal{B}$ lying on a rigid, flat substrate. We assume that the droplet consists of an incompressible fluid, so that it has a constant volume V. The boundary $\partial\mathcal{B}$ of $\mathcal{B}$ can be split as $\partial\mathcal{B}=\mathcal{S}\cup\mathcal{S}_*$, where the *free* surface $\mathcal{S}$ is in contact with the environment fluid, while the *adhering* surface $\mathcal{S}_*$ is in contact with the substrate. The surfaces $\mathcal{S}$ and $\mathcal{S}_*$ meet along the contact line $\mathcal{C}$, where three different phases coexist. The equilibrium configurations of the droplet $\mathcal{B}$ solve the Euler equation for the free-energy functional $\mathcal{F}$ defined by

$$\mathcal{F}[\mathcal{B}] := \gamma\int_{\mathcal{S}} da + (\gamma - w)\int_{\mathcal{S}_*} da + \tau\int_{\mathcal{C}} ds, \tag{1}$$

where γ is the *surface tension* associated with the interface $\mathcal{S}$ between the droplet and surrounding fluid, w is the *adhesion potential*, which characterizes the affinity between the droplet and substrate, and τ is the *line tension* introduced to account for the excess free energy concentrated along the contact line $\mathcal{C}$. In Eq. (1), a denotes the area measure and s is the arclength. At variance with γ and w, which are both positive, the line tension τ can be either positive or negative: the very objective of this paper is to study how the sign of τ affects the stability of the equilibria of $\mathcal{B}$.

In taking Eq. (1) as the free energy of the droplet $\mathcal{B}$, we are making several assumptions. We neglect body forces like gravity, and since w is constant, we also assume that the substrate is chemically homogeneous. We also assume that the line tension does not depend on the geometry of the contact line. While dropping any of these hypotheses has no effect on the validity of the methods we employ, assuming them contribute to simplify computations significantly.

The Euler equation associated with Eq. (1) has been derived countless times [10]: it requires the free surface $\mathcal{S}$ to have constant mean curvature. Since the contact line is not fixed, the following natural boundary condition, which generalizes the classical Young equation, holds along $\mathcal{C}$:

$$\gamma\cos\vartheta_c + \gamma - w - \tau\kappa_g^* = 0. \tag{2}$$

Here ϑ_c is the *contact angle*—that is, the angle between the droplet's and substrate's conormal unit vectors at the contact line $\mathcal{C}$ (see Fig. 1)—and κ_g^* is the geodesic curvature of $\mathcal{C}$, thought of as a curve on the substrate $\mathcal{S}^*$. The reader should heed that in [7] the contact angle was chosen as π-ϑ_c.

Among surfaces $\mathcal{S}$ with constant mean curvature, we focus our attention on spherical caps of radius R. As a further simplification, we assume that the substrate is *flat*, whence it follows that the contact line $\mathcal{C}$ is a circle with radius $R\sin\vartheta_c$ and with geodesic curvature on $\mathcal{S}^*$ (see, e.g., p. 249 of [15]):

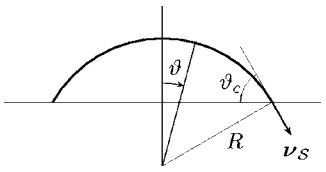

FIG. 1. Cross section of a spherical droplet with radius R lying on a flat, homogeneous substrate. The angle ϑ denotes the colatitude on the droplet's surface, and ϑ_c is the contact angle—that is, the angle between the droplet's and substrate's conormals.

$$\kappa_g^* = -\frac{1}{R \sin \vartheta_c}.$$

Finally, the volume V of the droplet $\mathcal{B}$ depends only on R and ϑ_c:

$$V = \frac{\pi R^3}{3}[2 + (\cos \vartheta_c)^3 - 3 \cos \vartheta_c]. \tag{3}$$

The dependence of κ_g^* on R and ϑ_c, which are further related through Eq. (3), makes it nontrivial resolving Eq. (2).

For future use, it is expedient to recast Eq. (2) in a dimensionless form. To this end, we note that for $(w-\gamma)/\gamma \in [-1,1]$ it is possible to define the *bare* contact angle ϑ_c^0 as

$$\cos \vartheta_c^0 := \frac{w-\gamma}{\gamma}. \tag{4}$$

Hence, ϑ_c^0 represents the contact angle at equilibrium, in the absence of line tension. The line tension τ introduces a typical length scale $|\xi|$, where

$$\xi := \frac{\tau}{\gamma}. \tag{5}$$

The ratio between ξ and the typical size of the droplet plays a major role in our analysis. The dimensionless ratios

$$\varepsilon := \frac{\xi}{R} \tag{6}$$

and

$$\tau_* := \frac{\xi}{\sqrt[3]{3V/\pi}} \tag{7}$$

will be used repeatedly in the sequel. For ease of the reader, we note that τ_* is noting but the dimensionless line tension $\bar{\tau}$ introduced by Widom in [7]. It should be noted that ξ, ε, and τ_* have the same sign as the line tension τ. By using Eqs. (4)–(7) we rephrase Eqs. (2) and (3) as

$$\varepsilon = \sin \vartheta_c(\cos \vartheta_c^0 - \cos \vartheta_c) =: \varepsilon_1(\vartheta_c, \vartheta_c^0), \tag{8a}$$

$$\varepsilon = \tau_* \sqrt[3]{2 + (\cos \vartheta_c)^3 - 3 \cos \vartheta_c} =: \varepsilon_2(\vartheta_c, \tau_*), \tag{8b}$$

provided that $\vartheta_c \in (0, \pi)$. Excluding $\vartheta_c = 0$ and $\vartheta_c = \pi$ means that we are in a partial wetting regime, away from both the wetting transition ($\vartheta_c = 0$) and the drying transition ($\vartheta_c = \pi$).

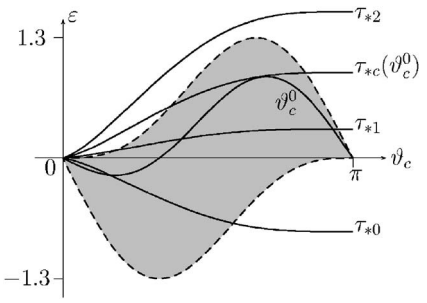

FIG. 2. Graphical solution of system (8), for a given value of ϑ_c^0. The admissible region $\mathcal{A}$ (in gray) has been plotted together with the curve $\varepsilon_1(\vartheta_c, \vartheta_c^0)$ and several curves in the family $\varepsilon_2(\vartheta_c, \tau_*)$. When $\tau_* \in [0, \tau_{*c}(\vartheta_c^0))$ (e.g., the curve $\tau_* = \tau_{*1}$), two acceptable equilibria exist, while no equilibrium exists for $\tau_* > \tau_{*c}(\vartheta_c^0)$ (e.g., the curve $\tau_* = \tau_{*2}$). At $\tau_* = \tau_{*c}(\vartheta_c^0)$ the two equilibria coalesce into a single equilibrium solution. When τ_* is negative (e.g., the curve $\tau_* = \tau_{*0}$), only one equilibrium exists. In $\mathcal{A}$, ε ranges within the interval $[-1.3, 1.3]$.

The function $\varepsilon_1(\vartheta_c, \vartheta_c^0)$ depends continuously on the bare contact angle ϑ_c^0, and $\varepsilon_2(\vartheta_c, \tau_*)$ depends continuously on τ_*. When ϑ_c^0 ranges in $[0, \pi]$, the curves $\varepsilon_1(\vartheta_c, \vartheta_c^0)$ span the shaded region $\mathcal{A}$ in Fig. 2, with the upper curve corresponding to $\vartheta_c^0 = 0$ and the lower curve to $\vartheta_c^0 = \pi$. We also note that the slope of $\varepsilon_1(\vartheta_c, \vartheta_c^0)$ at $\vartheta_c = 0$ is nonpositive, being zero only if $\vartheta_c^0 = 0$. The graphs of all functions in the family $\varepsilon_2(\vartheta_c, \tau_*)$ pass through the origin of the $(\vartheta_c, \varepsilon)$ plane and satisfy $\lim_{\vartheta_c \to 0} \varepsilon_2'(\vartheta_c, \tau_*) = 0$, where a prime stands for differentiation with respect to ϑ_c. If $\tau_* > 0$, the functions $\varepsilon_2(\vartheta_c, \tau_*)$ are monotonically increasing in ϑ_c, while they are monotonically decreasing in ϑ_c if $\tau_* < 0$. Whenever the graph of a function $\varepsilon_2(\vartheta_c, \tau_*)$ lies inside $\mathcal{A}$, there is at least one value of ϑ_c^0 that solves Eqs. (8). Conversely, for every point P in $\mathcal{A}$, there is at least a pair $(\bar{\vartheta}_c^0, \bar{\tau}_*)$ such that the graphs of $\varepsilon_1(\vartheta_c, \bar{\vartheta}_c^0)$ and $\varepsilon_2(\vartheta_c, \bar{\tau}_*)$ intersect at P and Eqs. (8) are solved.

The pair $\vartheta_c = 0$, $\varepsilon = 0$ always solves Eqs. (8), but this is a spurious solution arising from the way Eq. (8a) was obtained from Eq. (2). When $\tau_* > 0$ and the bare contact angle has a prescribed value ϑ_c^0, two solutions of Eq. (8a) exist as long as τ_* ranges in the interval $[0, \tau_{*c}(\vartheta_c^0)]$, where $\tau_{*c}(\vartheta_c^0)$ is determined by the condition that $\varepsilon_1'(\vartheta_c, \vartheta_c^0) = \varepsilon_2'(\vartheta_c, \tau_{*c}(\vartheta_c^0))$ for ϑ_c solving Eqs. (8). If $\tau_* > \tau_{*c}(\vartheta_c^0)$, Eqs. (8) have no solution, and so no equilibrium exists. This shows that even in a simple geometry, adding the line tension makes the modified Young equation nontrivial. When $\tau_* < 0$, a single solution of Eqs. (8) exists for any prescribed value of ϑ_c^0, as can easily be proved by noting that $\varepsilon_1(0, \vartheta_c^0) = \varepsilon_1(\pi, \vartheta_c^0) = 0$ and $\varepsilon_1'(0, \vartheta_c^0) < 0$, whereas the function $\varepsilon_2(\vartheta_c, \tau_*)$, which is monotonically decreasing in ϑ_c, obeys the limits $\lim_{\vartheta_c \to 0} \varepsilon_2(\vartheta_c, \tau_*) = 0$ and $\lim_{\vartheta_c \to 0} \varepsilon_2'(\vartheta_c, \tau_*) = 0$.

Figure 2 shows the possible scenarios outlined here, for a prescribed value of ϑ_c^0.

We finally obtain from Eq. (8a) that the equilibrium contact angle ϑ_c is larger than the bare contact angle ϑ_c^0 when the line tension is positive, whereas it is smaller than ϑ_c^0 when the line tension is negative. We also heed that, by Eq.

(8b), in the limit where the line tension is negative and divergent and so $\tau_* \to -\infty$, the equilibrium contact angle migrates towards 0. In the next section we will study the effects of line tension on the stability of the equilibrium solutions described here.

III. STABILITY

To obtain the Euler equation and the generalized Young's equation (2) governing the equilibrium shape of the droplet $\mathcal{B}$ we computed the first variation $\delta\mathcal{F}$ of the functional $\mathcal{F}$ by perturbing the points p on $\mathcal{B}$ as follows [10]:

$$p \mapsto p_\varepsilon := p + \epsilon \boldsymbol{u}, \tag{9}$$

and then requiring

$$\delta\mathcal{F}[\boldsymbol{u}] := \left.\frac{d\mathcal{F}[\boldsymbol{u}]}{d\epsilon}\right|_{\epsilon=0} = 0.$$

To assess the local stability of an equilibrium configuration, the sign of the second variation

$$\delta^2\mathcal{F} := \left.\frac{d^2\mathcal{F}[\boldsymbol{u}]}{d\epsilon^2}\right|_{\epsilon=0}$$

needs also to be evaluated. In [10] we proved that, in general, the perturbation (9) does not keep the constraints imposed on the problem up to second order in ϵ. In particular, we pointed out that, to account properly for the gliding of a droplet on an arbitrarily curved substrate, a point p in $\mathcal{B}$ must be mapped onto

$$p_\epsilon := p + \epsilon \boldsymbol{u} + \epsilon^2 \boldsymbol{v}, \tag{10}$$

with the fields $\boldsymbol{u}$ and $\boldsymbol{v}$ constrained to obey

$$\boldsymbol{u}\cdot\boldsymbol{\nu}_* = 0 \quad \text{and} \quad \boldsymbol{v}\cdot\boldsymbol{\nu}_* = -\frac{1}{2}\boldsymbol{u}\cdot(\boldsymbol{\nabla}_s\boldsymbol{\nu}_*)\boldsymbol{u} \quad \text{on } \mathcal{S}_*, \tag{11}$$

where $\boldsymbol{\nu}_*$ is the outer unit normal vector to the substrate and $\boldsymbol{\nabla}_s\boldsymbol{\nu}_*$ is its surface gradient. While the field $\boldsymbol{v}$ does not affect the first variation, it does affect the second variation: in particular, the use of $(11)_2$ together with the equilibrium equations makes it possible to write the second variation as a quadratic functional depending only upon the component $u := \boldsymbol{u}\cdot\boldsymbol{\nu}$ of the field $\boldsymbol{u}$ along the outer unit normal vector $\boldsymbol{\nu}$ to the free surface $\mathcal{S}$.

As usual, once the second variation $\delta^2\mathcal{F}$ is known, the local stability of an equilibrium configuration is guaranteed by minimizing it on the set

$$\int_{\mathcal{S}} u^2 da = 1 \tag{12}$$

and by requiring its minimum to be positive. Besides the constraint (12), the perturbation u must preserve the volume of the droplet and so it must also obey the requirement

$$\int_{\mathcal{S}} u da = 0. \tag{13}$$

The integral constraints (12) and (13) are accounted for by introducing suitable multipliers $-\frac{1}{2}\mu$ and ϱ, and then finding the minimum of

$$F[u] := \frac{1}{2}\int_{\mathcal{S}} \{|\nabla_s u|^2 + \alpha u^2\} da + \varrho\int_{\mathcal{S}} u da - \frac{1}{2}\mu\int_{\mathcal{S}} u^2 da + \frac{1}{2}\int_{\mathcal{C}} \{\xi u_{s*}'^2 - \beta u_{s*}^2\} ds, \tag{14}$$

where a prime now stands for differentiation with respect to the arclength s along $\mathcal{C}$. In Eq. (14),

$$\alpha := 2K - H^2, \tag{15}$$

where H and K are the total and Gaussian curvatures of $\mathcal{S}$, and u_{s*} is related to u through

$$u_{s*} = \frac{u}{\sin\vartheta_c}.$$

Finally,

$$\gamma\beta := \tau(K^* + \kappa_g^{*2}) + \gamma[H^*\sin\vartheta_c + H\cos\vartheta_c\sin\vartheta_c + \kappa_g(\sin\vartheta_c)^2], \tag{16}$$

where H^* and K^* are the total and Gaussian curvatures of $\mathcal{S}_*$, and κ_g and κ_g^* are the geodesic curvatures of the contact line $\mathcal{C}$, regarded as a curve on $\mathcal{S}$ and $\mathcal{S}_*$, respectively. The definitions (15) and (16) are indeed special cases of the general definitions given in [10], where the effects of inhomogeneities in the chemical composition of the substrate, nonconstant line tension, and geometric microstructures were also taken into account.

For a spherical cap $\mathcal{S}$ of radius R lying on a flat substrate, $H=2/R$, $K=1/R^2$, $H^*=0$, and $K^*=0$; moreover, along the circular contact line $\mathcal{C}$, $\kappa_g=-\cot\vartheta_c/R$ and $\kappa_g^*=-1/R\sin\vartheta_c$. By the same analysis as in [10], the equilibrium equations for $F[u]$ read as

$$\Delta_s u + \left(\mu + \frac{2}{R^2}\right)u = \varrho \quad \text{on } \mathcal{S} \tag{17}$$

and

$$\left[\frac{\partial u}{\partial\vartheta} - \frac{\varepsilon}{(\sin\vartheta_c)^4}\frac{\partial^2 u}{\partial\varphi^2} - \frac{1}{(\sin\vartheta_c)^2}\left(\frac{\varepsilon}{(\sin\vartheta_c)^2} + \sin\vartheta_c\cos\vartheta_c\right)u\right]\Bigg|_{\vartheta=\vartheta_c} = 0 \quad \text{along } \mathcal{C}, \tag{18}$$

where the differential operator

$$\Delta_s := \frac{1}{R^2}\frac{\partial^2}{\partial\vartheta^2} + \frac{1}{R^2}\cot\vartheta\frac{\partial}{\partial\vartheta} + \frac{1}{(R\sin\vartheta)^2}\frac{\partial^2}{\partial\varphi^2} \tag{19}$$

is the surface Laplacian on the sphere, expressed in terms of the colatitude $\vartheta\in[0,\vartheta_c]$ and the azimuth $\varphi\in[0,2\pi)$ (see Fig. 1). The minimum eigenvalue $\mu_{\min}$ of Eqs. (17) and (18) coincides with the minimum value of $\delta^2\mathcal{F}$ on the set (12): a

configuration is unstable if $\mu_{\min}$ is negative and locally stable if $\mu_{\min}$ is positive.

To find $\mu_{\min}$ or, at least, to determine its sign, it is expedient to expand the solution $\bar{u}$ of the homogenous problem

$$\Delta_s \bar{u} + (\mu + 2)\bar{u} = 0 \quad \text{on } \mathcal{S} \tag{20}$$

as

$$\bar{u} = \sum_{m=0}^{\infty} a_m u_m(\vartheta)\mathrm{trig}(m\varphi), \tag{21}$$

where

$$\mathrm{trig}(m\varphi) := \begin{cases} \sin(m\varphi) \text{ or } \cos(m\varphi) & \text{if } m \neq 0, \\ 1 & \text{if } m = 0, \end{cases}$$

and $a_m \in \mathbb{R}$ are the coefficients of the expansion. In Eq. (20), the factor R^{-2} in front of Δ_s in Eq. (19) has been dropped by rescaling μ to R^2. We insert the expansion (21) into Eq. (20) and conclude that, for every value of m, the function $u_m(\vartheta)$ solves the equation

$$\frac{1}{\sin\vartheta}\frac{d}{d\vartheta}\left[\sin\vartheta\frac{du_m}{d\vartheta}\right] + \left[\mu + 2 - \left(\frac{m}{\sin\vartheta}\right)^2\right]u_m = 0. \tag{22}$$

The solution of Eq. (22) that is bounded everywhere on $\mathcal{S}$ is the associated Legendre function of the first kind $P_\nu^m(\cos\vartheta)$, where the index ν is related to μ by

$$\nu(\nu+1) = \mu + 2. \tag{23}$$

Equation (22) can also be solved for complex values of ν. Since the product $\nu(\nu+1)$ is invariant under the transformation $\nu \mapsto -(1+\nu)$, we can restrict our attention to the values of ν with real part $\mathrm{Re}(\nu) \geqslant -\frac{1}{2}$. Moreover, since the product $\nu(\nu+1)$ is left unchanged when the imaginary part $\mathrm{Im}(\nu)$ of ν is changed into its opposite, we can also assume $\mathrm{Im}(\nu) \geqslant 0$. Equation (22) needs to be solved only when μ is real—that is, for either

$$\mathrm{Im}(\nu) = 0 \quad \text{or} \quad \mathrm{Re}(\nu) = -\frac{1}{2}.$$

Collecting all this information, we conclude that the parameter ν ranges in the set $\mathcal{I}$ of the complex ν plane shown in Fig. 3, formally defined as

$$\mathcal{I} := \left\{\nu \in \left[-\frac{1}{2} + i0, -\frac{1}{2} + i\infty\right) \cup \left[-\frac{1}{2}, +\infty\right)\right\}.$$

By Eq. (23), instability occurs for $\mathrm{Re}(\nu) < 1$—that is, for

$$\nu \in \mathcal{U} := \left\{\left[-\frac{1}{2} + i0, -\frac{1}{2} + i\infty\right) \cup \left[-\frac{1}{2}, 1\right)\right\}. \tag{24}$$

The associated Legendre functions $P_\nu^m(\cos\vartheta)$ are also called *spherical* functions when ν is real and *conical* functions when $\nu = -\frac{1}{2} + i\lambda$, with $\lambda > 0$. Unstable modes with a real ν will be referred to as the *spherical modes*; unstable modes with complex ν will be referred to as the *conical modes*.

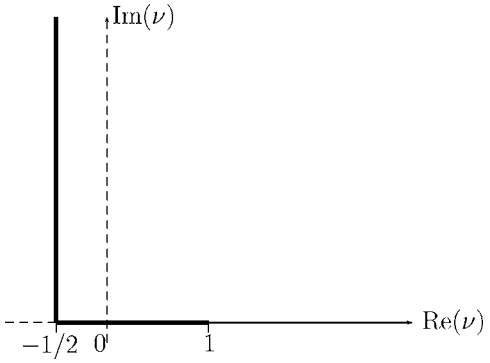

FIG. 3. Complex values of ν relevant to our analysis. The real and imaginary axes of the complex ν plane are dashed lines; the set $\mathcal{I}$ is the solid line, whose thicker part represents the subset $\mathcal{U}$ corresponding to negative values of the multiplier μ and, hence, to unstable equilibria.

The solution u of Eq. (17) with ϱ rescaled to R^2 differs from $\bar{u}$ by a constant c related to the multipliers ϱ and μ through

$$(\mu + 2)c = \nu(\nu+1)c = \varrho, \tag{25}$$

provided that $\mu \neq -2$ or, equivalently, $\nu \neq 0$. In general, the function u must also satisfy the incompressibility constraint (13), which now reads as

$$\int_0^{\vartheta_c}\int_0^{2\pi} u(\vartheta,\varphi)\sin\vartheta\, d\vartheta\, d\varphi = 0. \tag{26}$$

In a modal analysis, where conditions are sought that make a specific mode unstable, the constraint (26) is adjusted mode by mode, by adding to the function

$$u_m(\vartheta,\varphi) := P_\nu^m(\cos\vartheta)\mathrm{trig}(m\varphi), \quad m \in \mathbb{N}, \tag{27}$$

a constant $c(\vartheta_c, \nu, m)$ that makes Eq. (26) satisfied so that ϱ, now depending on ϑ_c, ν, and m, follows from Eq. (25) for all ν but $\nu = 0$, a case which will be recovered below as a limiting case. (An independent study of the case $m=0$, $\nu=0$ is presented for completeness in Appendix A.)

The factor $\mathrm{trig}(m\varphi)$ guarantees that $u_m(\vartheta,\varphi)$ automatically obeys Eq. (26) when $m > 0$, and so both $c(\vartheta_c,\nu,m)$ and the corresponding value of ϱ vanish for all $m > 0$. When $m = 0$, to determine c we proceed as follows. First, we heed that [see Eq. (7.8.3) of [16]]

$$P'_{\nu+1}(x) - xP'_\nu(x) = (\nu+1)P_\nu(x), \tag{28}$$

where the superscript 0 in the Legendre functions is omitted for brevity and a prime stands for differentiation with respect to the argument. Second, since

$$\int_0^{\vartheta_c}\int_0^{2\pi} P_\nu(\cos\vartheta)\sin\vartheta\, d\vartheta\, d\varphi = 2\pi\int_{x_c}^{1} P_\nu(x)dx,$$

where $x_c := \cos\vartheta_c$, by integrating in Eq. (28) by parts and recalling that $P_\nu(1) = 1$ for all values of ν, we obtain

$$\int_0^{\vartheta_c}\int_0^{2\pi} P_\nu(\cos\vartheta)\sin\vartheta\, d\vartheta d\varphi = \frac{\cos\vartheta_c P_\nu(\cos\vartheta_c) - P_{\nu+1}(\cos\vartheta_c)}{\nu} \quad \text{if } \nu \neq 0.$$

Hence, for each integer m we replace u in Eqs. (17) and (26) with $u_m(\vartheta,\varphi)+c(\vartheta_c,\nu,m)$, where the constant $c(\vartheta_c,\nu,m)$ is given by

$$c(\vartheta_c,\nu,m) := \begin{cases} 0 & \text{if } m \neq 0, \\ -\dfrac{\cos\vartheta_c P_\nu(\cos\vartheta_c) - P_{\nu+1}(\cos\vartheta_c)}{(1-\cos\vartheta_c)\nu} & \text{if } m = 0, \end{cases} \tag{29}$$

and then we solve Eq. (18) in terms of ε, which in turn becomes a function $\varepsilon_\nu^m(\vartheta_c)$ of the contact angle ϑ_c, parametrized in ν and m. A straightforward substitution yields

$$\varepsilon_\nu^m(\vartheta_c) = -(\sin\vartheta_c)^4 \frac{\left(\cot\vartheta_c P_\nu^m(\cos\vartheta_c) - \left.\dfrac{\partial P_\nu^m(\cos\vartheta)}{\partial\vartheta}\right|_{\vartheta_c}\right)}{(1-m^2)P_\nu^m(\cos\vartheta_c)} \quad \text{if } m \neq 0,1, \tag{30a}$$

$$\varepsilon_\nu^m(\vartheta_c) = -(\sin\vartheta_c)^4 \frac{\left(\cot\vartheta_c (P_\nu(\cos\vartheta_c) + c(\vartheta_c,\nu,0)) - \left.\dfrac{\partial P_\nu(\cos\vartheta)}{\partial\vartheta}\right|_{\vartheta_c}\right)}{c(\vartheta_c,\nu,0) + P_\nu(\cos\vartheta_c)} \quad \text{if } m = 0. \tag{30b}$$

Modes with $m=1$ are excluded in Eqs. (30) because, as shown in Appendix B, they satisfy the boundary condition (18) only for $\nu=1$. Thus, these modes are marginally stable, as $\mu=0$. This should not come as a surprise, since the function $P_1^1(\cos\vartheta)\mathrm{trig}\varphi = \sin\vartheta\,\mathrm{trig}\varphi$ is proportional to the projection along the droplet's normal of a uniform translation along the flat substrate. Hence, the marginal modes $m=1$ simply reflect the invariance under translations of the free-energy functional, already noted by Sekimoto, Oguma, and Kawasaky [13].

By plotting the graphs of the functions $\varepsilon_\nu^m(\vartheta_c)$, we can decide whether the equilibrium configurations found in Sec. II are locally stable or not, with respect to specific modes. The points of the admissible region $\mathcal{A}$ that also belong to the graph of a function $\varepsilon_\nu^m(\vartheta_c)$ with $\mathrm{Re}\,\nu<1$ correspond to unstable equilibria of the droplet.

So far, our modal analysis is independent of the sign of the line tension. Since different outcomes are expected for different signs, we split our study into two parts, starting from the case where the line tension is negative.

A. Negative line tension

When the line tension is negative, the droplet is expected to be unstable against modes that increase sufficiently the length of its contact line. Our development below will indeed make this expectation quantitative. This, however, does not mean that all modes are unstable. Actually, it is shown in Appendix B that every configuration $(\vartheta_c,\varepsilon)$ is stable against the mode $m=0$ for an appropriate $\nu>1$. The mode $m=0$ will hereafter be disregarded since, as shown in the next subsection, it becomes unstable only for positive line tensions. Moreover, we already know that the modes $m=1$ correspond to rigid translations. Our analysis will thus concern only the functions $\varepsilon_\nu^m(\vartheta_c)$ for $m\geqslant 2$.

Equation (30a) can be recast as [see Eq. (C1) in Appendix C]

$$\varepsilon_\nu^m(\vartheta_c) = \frac{[(m+\nu)P_{-1+\nu}^m(\cos\vartheta_c) - (\nu-1)\cos\vartheta_c P_\nu^m(\cos\vartheta_c)]\sin^3\vartheta_c}{(m^2-1)P_\nu^m(\cos\vartheta_c)}. \tag{31}$$

For a fixed value of m, we select two arbitrary real values of ν—say, ν_1 and $\nu_2>\nu_1$, with ν_1 and ν_2 different from 0 and 1—and we draw the graphs of the functions $\varepsilon_{\nu_1}^m(\vartheta_c)$ and $\varepsilon_{\nu_2}^m(\vartheta_c)$: the cases $\nu=0$ and $\nu=1$ need to be momentarily excluded, since the associated Legendre function $P_\nu^m(\cos\vartheta_c)$ is identically zero when ν is an integer less than m, and so Eq. (31) makes no sense. Since the function $\varepsilon_\nu^m(\vartheta_c)$ depends continuously on ν, each point of the $(\vartheta_c,\varepsilon)$ plane between

the graphs of $\varepsilon_{\nu_1}^m(\vartheta_c)$ and $\varepsilon_{\nu_2}^m(\vartheta_c)$ also belongs to the graph of a function $\varepsilon_\nu^m(\vartheta_c)$ for some $\nu \in (\nu_1, \nu_2)$. By repeating this argument when m is varied and letting ν span the whole set $\mathcal{U}$ defined in Eq. (24), we find all pairs $(\vartheta_c, \varepsilon)$ that correspond to unstable equilibria, including both spherical and conical modes. The graph of $\varepsilon_\nu^m(\vartheta_c)$ approaches limiting curves when ν tends either to 0 or 1, though the corresponding limiting modes u_m fail to be in $L^2(\mathcal{S})$—that is, square summable on $\mathcal{S}$. By appropriately truncating these functions, it is possible to construct minimizing sequences in $L^2(\mathcal{S})$ on which $\delta^2\mathcal{F}$ converges to -2 and 0, which, by Eq. (25), are the values of μ corresponding to $\nu=0$ and $\nu=1$, respectively. In the former case, we can conclude that the curves $\varepsilon_0^m(\vartheta_c)$ are unstable, since $\delta^2\mathcal{F}$ attains negative values arbitrarily close to -2 on the minimizing sequence. In the latter case, we conclude that the curves $\varepsilon_1^m(\vartheta_c)$ are marginal, since $\delta^2\mathcal{F}$ remains positive on the minimizing sequence, though arbitrarily close to 0. In short, we find that for a given value of m the region below the marginal curve $\varepsilon_1^m(\vartheta_c)$ is covered by the curves $\varepsilon_\nu^m(\vartheta_c)$ with $\nu \in \mathcal{U}$. In more detail, the curves $\varepsilon_\nu^m(\vartheta_c)$ corresponding to spherical modes $\nu \in \left[-\frac{1}{2}, 1\right)$ lie above the curves $\varepsilon_{-(1/2)+i\lambda}^m(\vartheta_c)$ corresponding to conical modes: precisely, in Appendix D, we prove that all the points in the $(\vartheta_c, \varepsilon)$ plane below the curve $\varepsilon_{-1/2}^m(\vartheta_c)$ also belong to a curve $\varepsilon_{-(1/2)+i\lambda}^m(\vartheta_c)$ for some $\lambda > 0$. The continuous dependence of the functions $\varepsilon_\nu^m(\vartheta_c)$ on ν and the limit (D1) ensure that, for any prescribed value of m, the manifold $\{(\vartheta_c, \varepsilon) \,|\, \vartheta_c \in (0, \pi), \varepsilon < \varepsilon_1^m(\vartheta_c)\}$ is unstable against the m-indexed modes. Since $\mu_{\min}=0$ along the curves $\varepsilon_1^m(\vartheta_c)$, their intersections with $\mathcal{A}$ are marginal curves: they delimit the regions in $\mathcal{A}$ that are unstable against the m-indexed modes. It is proved in Appendix E that the marginal curves ε_1^m converge to the ϑ_c axis as m increases. Strictly speaking, only the unstable pairs $(\vartheta_c, \varepsilon)$ within the admissible set $\mathcal{A}$ matter, as they correspond to attainable equilibria. However, near the origin $\mathcal{A}$ is covered by the graphs of $\varepsilon_{-(1/2)+i\lambda}^m(\vartheta_c)$, with $\lambda \gg 1$. This explains why we look first for the unstable pairs $(\vartheta_c, \varepsilon)$ with negative ε and then we restrict the unstable manifold to $\mathcal{A}$. The interplay of spherical and conical modes in weaving the whole unstable manifold is illuminated in Ref. [17].

Figure 4 summarizes the stability analysis. Here, the marginal curves corresponding to several values of m have been plotted together with the admissible region $\mathcal{A}$. Whenever a pair $(\vartheta_c, \varepsilon)$ falls within the region Us below the lowermost marginal curve $\varepsilon_1^2(\vartheta_c)$, the droplet is unstable. In the region Rs above the curve $\varepsilon_1^2(\vartheta_c)$, equilibria are conditionally stable: for a given equilibrium configuration of the droplet, the smallest value m_{rs} of m for which the corresponding modes are unstable is an index of stability of the equilibrium configuration, a stability that we call *residual* as it results from the suppression of all unstable modes $m \geqslant m_{\mathrm{rs}}$. For a given point p in Rs, the marginal curves with $m \leqslant m_{\mathrm{rs}}$ lie below p, while those with $m > m_{\mathrm{rs}}$ lie above it. For $m_{\mathrm{rs}}=2$, the droplet is simply unstable. In Fig. 5 three different graphs of m_{rs} are plotted in terms of the dimensionless line tension τ_* for some values of the bare contact angle ϑ_c^0. All these graphs are necessarily discontinuous, and m_{rs} increases as τ_* approaches zero.

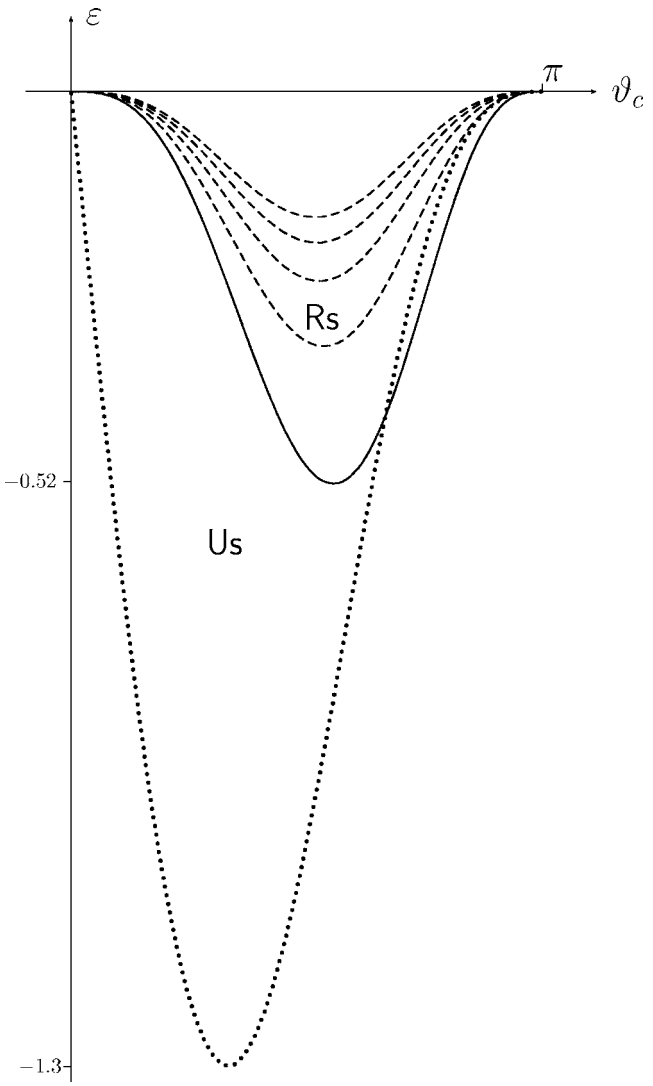

FIG. 4. Stability analysis for negative line tension. The dotted curve delimits the admissible region $\mathcal{A}$ in Fig. 2. The solid line is the marginal curve $\varepsilon_1^2(\vartheta_c)$, along which the minimum value of ε is $\varepsilon \approx -0.52$. In the region Us below $\varepsilon_1^2(\vartheta_c)$, equilibria are unstable regardless of the magnitude of the line tension. In the region Rs above $\varepsilon_1^2(\vartheta_c)$, equilibria are residually stable. The dashed curves in Rs are marginal curves corresponding to $m=3,4,5,6$, ordered upwards. For every point p in Rs, there exists a value m_{rs} of m such that all marginal curves with $m \leqslant m_{\mathrm{rs}}$ lie below p, while those with $m > m_{\mathrm{rs}}$ lie above it. Consequently, p represents an equilibrium stable against modes with $m \leqslant m_{\mathrm{rs}}$ and unstable against modes with $m > m_{\mathrm{rs}}$. In the limit where $m \to \infty$, the marginal curves tend towards the ϑ_c axis.

When the line tension is negative, the functional $\mathcal{F}$ in Eq. (1) is unbounded from below. No equilibrium configuration of $\mathcal{F}$ can be stable when m is large enough, because the perturbing modes make the contact line more and more wrinkled. Intuitively, upon increasing m, the typical length ℓ_m over which corrugations associated with the m-indexed modes manifest themselves decreases. When ℓ_m becomes smaller than the microscopic length ℓ_{mic}, the corresponding modes are inconsistent with our analysis, as they induce deformations of the droplets at length scales that lie beyond the

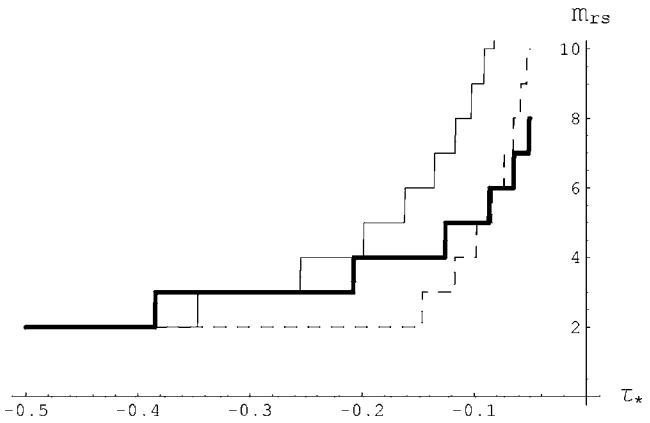

FIG. 5. The index m_{rs} of residual stability against the dimensionless line tension τ_*, when the bare contact angle ϑ_c^0 is $\pi/4$ (dashed line), $\pi/2$, or $3\pi/4$ (thick line). Two features are worth noting. First, when the magnitude of the (negative) line tension is large enough, $m_{\mathrm{rs}}=2$, meaning that all modes are unstable. Second, on approaching $\tau_*=0$, m_{rs} diverges, implying that the range of residual stability increases.

range of validity of the continuum model. Bounding ℓ_m from below, so as to ensure consistency to the model, is the same as bounding the index m of the allowed modes from above.

A formal definition of the typical length ℓ_m associated with the marginal mode

$$u_m^*(\vartheta,\varphi) := P_1^m(\cos\vartheta)\mathrm{trig}(m\varphi) \tag{32}$$

can be given as follows. Equation (32), which is for the marginal mode the same as Eq. (27) for the generic mode, describes a system of alternating bumps and dips on the spherical cap $\mathcal{S}$ with radius R representing the unperturbed equilibrium configuration of the droplet. The nodal set of u_m^*—that is, the set where u_m^* vanishes—is a network of parallels and meridians that delimit a tessellation of $\mathcal{S}$. The two shortest lengths associated with such a network are exhibited by the $2m$ spherical triangles that have a vertex in the pole of $\mathcal{S}$ where $\vartheta=0$. These triangles are isosceles with base

$$\ell_m := \frac{\pi R \sin\vartheta_0^m}{m} \tag{33}$$

and oblique side

$$s_m := R\vartheta_0^m,$$

where ϑ_0^m is either the smallest positive root of $P_1^m(\cos\vartheta)$ in $[0,\vartheta_c]$, when it exists, or ϑ_c, when the smallest positive root of $P_1^m(\cos\vartheta)$ lies outside $[0,\vartheta_c]$. For m sufficiently large, $\ell_m<s_m$ and Eq. (33) defines the shortest length associated with the marginal mode u_m^*.

To enforce our stability criterion the length ℓ_{rs} that corresponds through Eq. (33) to the index m_{rs} must be compared with ℓ_{mic}. If $\ell_{\mathrm{rs}}>\ell_{\mathrm{mic}}$, the drop is unstable because there are unstable modes compatible with the continuum model. If $\ell_{\mathrm{rs}}<\ell_{\mathrm{mic}}$, the drop is stable because all modes compatible with the continuum model are stable.

For $R=1$ μm, Widom [7] gave the estimate $|\tau_*|\approx 0.063$, based on experimentally reasonable values of surface and line tensions. It is clear from Fig. 5 that when $\tau_*\approx -0.063$ the index of residual stability is larger than 6 for all values of ϑ_c^0 plotted there. Taking, for example, $m_{\mathrm{rs}}=10$, we obtain $\ell_{\mathrm{rs}}\approx 0.1$ μm, which is larger than ℓ_{mic}, and so we conclude that this hypothetical drop would be unstable.

Figure 5 only conveys partial information, as each staircase is plotted for a fixed value of ϑ_c^0. To learn how m_{rs} depends on the constitutive parameters ϑ_c^0 and τ_* of the model, we need to interpret in terms of these the stability analysis performed in the $(\vartheta_c,\varepsilon)$ plane, where it was easier to solve Eqs. (17) and (18). This is achieved by finding a mapping

$$v:(\vartheta_c,\varepsilon)\mapsto(\cos\vartheta_c^0,\tau_*)$$

that maps solutions of Eqs. (8) into the $(\cos\vartheta_c^0,\tau_*)$ plane. We shall also refer to v as to the *reverse mapping*. To find the reverse mapping we solve Eqs. (8) with respect to $\cos\vartheta_c^0$ and τ_*, obtaining

$$\cos\vartheta_c^0(\vartheta_c,\varepsilon) = \frac{\varepsilon}{\sin\vartheta_c} + \cos\vartheta_c, \tag{34a}$$

$$\tau_*(\vartheta_c,\varepsilon) = \frac{\sqrt[3]{2+(\cos\vartheta_c)^3-3\cos\vartheta_c}}{\varepsilon}. \tag{34b}$$

Then, the image of the function $\varepsilon_\nu^m(\vartheta_c)$ is the parametric curve

$$v(\varepsilon_\nu^m(\vartheta_c)) = (\cos\vartheta_c^0(\vartheta_c,\varepsilon_\nu^m(\vartheta_c)),\tau_*(\vartheta_c,\varepsilon_\nu^m(\vartheta_c)))$$

obtained from Eqs. (34).

For a negative line tension, the reverse mapping is a one-to-one function as for a given pair $(\cos\vartheta_c^0,\delta)$ there is a unique pair $(\vartheta_c,\varepsilon)$ that solves Eqs. (8). For a positive line tension, the reverse mapping is a one-to-two function, whose branches give the bifurcation diagram we discuss in the next subsection. Figure 6 shows the curves that link ϑ_c^0 and τ_* for a given index m_{rs} of residual stability to be achieved. The values of m_{rs} considered here range from 2 to 100. For given ϑ_c^0 and τ_*, the index of residual stability associated with them can easily be estimated by identifying the curves in Fig. 6 that pass close to the point $(\cos\vartheta_c^0,-\log_{10}|\tau_*|)$. All the curves in Fig. 6 were obtained as reverse mappings of the curves $\varepsilon_1^{m_{\mathrm{rs}}}(\vartheta_c)$.

To show how the graphs in Fig. 6 can be employed in practice, we compute the value of τ_* from data obtained in [14] for the line tension of an octane droplet, close to the wetting transition. Using the values $\vartheta_c^0=9.5°$ and $\tau=-4.4\times10^{-10}$ N, measured at the temperature of 28 °C, and taking 1.4×10^{-5} m as a typical value of $\sqrt[3]{3V/\pi}$, obtained for octane from Fig. 4 of [14], we find $\tau_*=-0.13\times10^{-2}$. This and the other values of τ_* obtained from the negative values of τ reported in Table 1 of [14], for droplets on the same substrate at different temperatures, are displayed in Fig. 7.

Most of the experimental data are across the line with index of residual stability $m_{\mathrm{rs}}=50$. Thus, according to the theory presented here, for the droplets observed in [14] the index of residual stability is considerably higher than for the droplet envisaged by Widom [7]. The fact suggested in Fig. 7

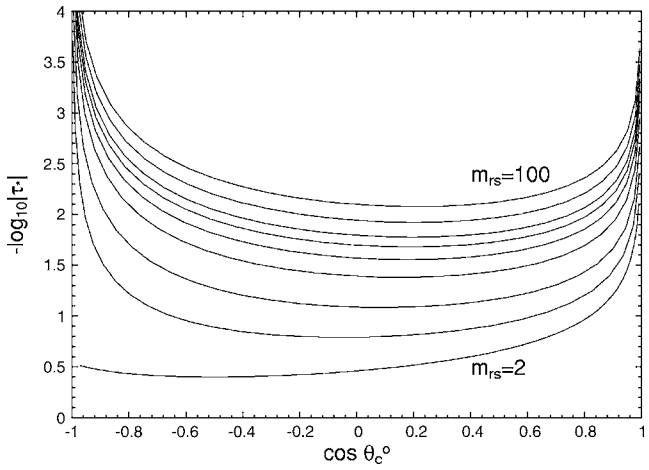

FIG. 6. Curves corresponding to different values of the index $m_{\rm rs}$ of residual stability. From the lower to the upper curve, $m_{\rm rs}=2,5,10,20,30,40,50,70,100$. The vertical axis reports $-\log_{10}\times|\tau_*|$, so that going upwards the line tension passes from higher, negative values to smaller, negative values. The curve $m=2$ marks the onset of residual stability: below it, no stable mode exists at all.

that droplets with different bare contact angles ϑ_c^0 have index of residual stability $m_{\rm rs}$ close to 50 may well be accidental, and different lengths $\ell_{\rm rs}$ may indeed correspond to similar indices $m_{\rm rs}$ when ϑ_c^0 changes. For illustrative purposes, we pick the data shown in Fig. 4 of [14] and compute the corresponding $\ell_{\rm rs}$ for $m=50$: taking $R\sin\vartheta_c\approx 35\ \mu$m and $\vartheta_c\simeq 5°$, we obtain $\ell_{\rm rs}\approx 40$ nm, which we reckon to be less than $\ell_{\rm mic}$. Thus, the droplets observed by Wang, Betelu, and Law [14] are stable according to our criterion and their measures of negative line tensions appear to be highly reliable.

B. Positive line tension

We proved in the preceding subsection that all modes $m\geqslant 2$ make the droplet unstable only when the line tension,

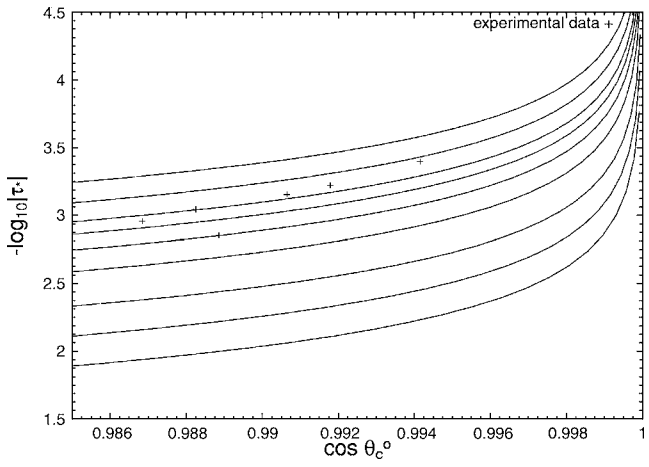

FIG. 7. The experimental data obtained in [14] are plotted against the curves with constant index of residual stability illustrated in Fig. 6. The experimental points are represented by crosses and $m_{\rm rs}=2,5,10,20,30,40,50,70,100$, from the lower to the upper curve. Most experimental points fall across the curve with $m_{\rm rs}=50$.

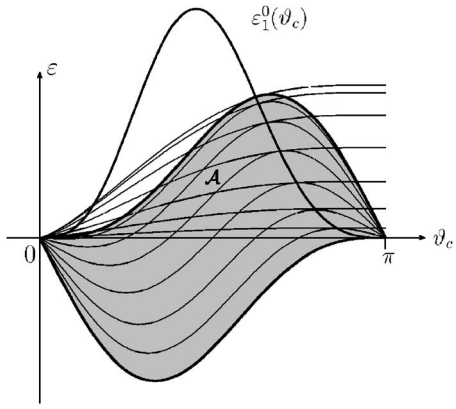

FIG. 8. The marginal curve $\varepsilon_1^0(\vartheta_c)$ divides the admissible set $\mathcal{A}$ into two parts. Only the part below the graph of $\varepsilon_1^0(\vartheta_c)$ is stable. The thin lines are graphs of the functions $\varepsilon_1(\vartheta_c,\vartheta_c^0)$ and $\varepsilon_2(\vartheta_c,\tau_{*c}(\vartheta_c^0))$ defined in Eqs. (8), for several values of ϑ_c^0. When $\tau_*=\tau_{*c}(\vartheta_c^0)$, the two equilibria coalesce into one another and so $\varepsilon_1(\vartheta_c,\vartheta_c^0)$ and $\varepsilon_2(\vartheta_c,\tau_{*c}(\vartheta_c^0))$ have a common tangent. Here we see that the marginal curve $\varepsilon_1^0(\vartheta_c)$ passes through all these tangent points.

and so ε, is negative, as the graphs of the curves $\varepsilon_\nu^m(\vartheta_c)$ lie in the negative quadrant $\{(\vartheta_c,\varepsilon)\,|\,\vartheta_c\in[0,\pi],\varepsilon<0\}$. Moreover, modes with $m=1$ and $\nu=1$ are associated with rigid translations of the droplet for all values of the line tension. Hence, when the line tension is positive, only the modes with $m=0$, which are stable for negative line tensions, can become unstable, and indeed they do, as we now proceed to show.

The modes $m=0$ are described by the functions $\varepsilon_\nu^0(\vartheta_c)$ defined in Eq. (30b), with $c(\vartheta_c,\nu,0)$ given by $(29)_2$. By reasoning as in Sec. III A, we conclude that the set of the $(\vartheta_c,\varepsilon)$ plane bounded by the graphs of $\varepsilon_1^0(\vartheta_c)$ and $\varepsilon_{-1/2}^0(\vartheta_c)$ corresponds to unstable equilibria, with $\varepsilon_1^0(\vartheta_c)$ playing the role of marginal curve. It is proved in Appendix F that the set of the $(\vartheta_c,\varepsilon)$ plane above the graph of $\varepsilon_{-1/2}^0(\vartheta_c)$ contains the graph of $\varepsilon_{-(1/2)+i\lambda}^0(\vartheta_c)$, for some positive value of λ. Finally, by the same arguments in Sec. III A, we conclude that the set below the graph of $\varepsilon_1^0(\vartheta_c)$ corresponds to locally stable equilibria, since there the minimum value of μ is positive. Hence, when the line tension is positive, the curve $\varepsilon_1^0(\vartheta_c)$ is a marginal curve.

As already shown in Sec. II for a given value ϑ_c^0 of the bare contact angle, there is a critical value $\tau_{*c}(\vartheta_c^0)$ of τ_* such that, if $\tau_*\in[0,\tau_{*c}(\vartheta_c^0))$, there are two equilibria, and if $\tau_*>\tau_{*c}(\vartheta_c^0)$, there is none.

Figure 8 shows the graph of the marginal curve superimposed to the admissible set $\mathcal{A}$: only the subset of $\mathcal{A}$ below the curve $\varepsilon_1^0(\vartheta_c)$ contains stable equilibria: for given values of ϑ_c^0 and τ_*, when two equilibria exist, only the one with the lowest value of ϑ_c is stable. We also note that the two equilibria coalesce along the marginal curve $\varepsilon_1^0(\vartheta_c)$.

The modes that mark the transition from stable to unstable equilibria have normal component u proportional to $\cos\vartheta+c$. Hence, Eq. (10) maps spheres onto spheres, as it should since the stability threshold found here agrees with Widom's [7], though perturbations preserving the spherical shape of the droplet were not the only ones considered in our analysis.

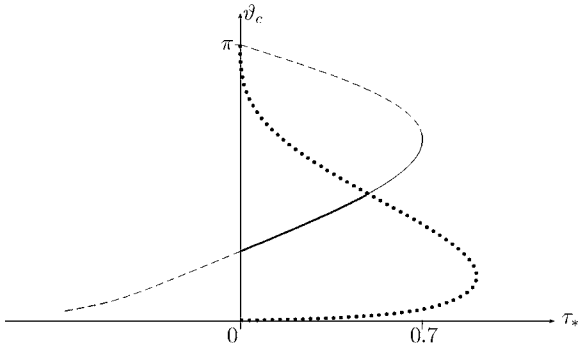

FIG. 9. Bifurcation diagram showing the stability of equilibria in terms of the dimensionless line tension τ_*, when the bare contact angle ϑ_c^0 is $\pi/3$. Solutions are parametrized by their contact angle ϑ_c. Dashed lines correspond to unstable equilibria. Solid lines correspond to stable equilibria: both locally stable (thin line) and globally stable (thick line). The dotted line marks the first-order drying transition.

It is remarkable that the restricted stability analysis of Widom [7] delivers the correct result, at least for positive line tensions. Figure 9 contains the essential results of our stability analysis for positive line tension: a bifurcation diagram is illustrated for a given value of the bare contact angle ϑ_c^0.

For positive values of τ_*, the local stability of a droplet is completely determined by the preceding analysis. To explore the global stability, we compare as in [7] the energy of a sessile droplet with that of a completely detached sphere and that of a completely wetted substrate. By setting

$$x_0 := \cos\vartheta_c^0 \quad \text{and} \quad x := \cos\vartheta_c$$

and using the definition of τ_* as in Eq. (7), as well as the volume constraint (3), we can recast the modified Young's equation (2) in the form

$$\tau_* = (x_0 - x)(2+x)^{-1/3}(1-x)^{-1/6}(1+x)^{1/2}, \tag{35}$$

which coincides with Eq. (12) of [7], provided that x and x_0 are changed to their opposite to accommodate the different definitions of the contact angle. By inserting Eq. (35) into the dimensionless free energy

$$F := \frac{\mathcal{F}}{2\pi\gamma\left(\frac{3V}{\pi}\right)^{2/3}},$$

for a sessile droplet, we obtain

$$F_s(x) = (1-x)^{-1/3}(2+x)^{-2/3}\left[1 + (1+x)\left(\frac{x_0}{2} - x\right)\right].$$

To find the locus in the (ϑ_c, τ_*) plane where F_s coincides with the free energy of a completely detached sphere, we need to solve the equation [cf. Eq. (16) of [7]]

$$(1-x)^{-1/3}(2+x)^{-2/3}\left[1 + (1+x)\left(\frac{x_0}{2} - x\right)\right] = 2^{-1/3}, \tag{36}$$

where the right-hand side is the dimensionless free energy of a detached sphere of fixed volume V. Equations (35) and (36) determine the locus in the (ϑ_c, τ_*) plane where a first-order drying transition occurs: its analytic expression readily follows by inserting into Eq. (35) the value of x_0 obtained from Eq. (36). It is shown as a dotted curve in Fig. 9.

The limiting value F_w of the dimensionless free energy of a droplet that completely wets the substrate is $+\infty$ for $\cos\vartheta_c^0 < 1$ and any line tension. Still $F_w = +\infty$ for $\cos\vartheta_c^0 = 1$ and a positive line tension: this shows that a positive line tension never promotes complete wetting. On the contrary, $F_w = -\infty$ for $\cos\vartheta_c^0 = 1$ and a negative line tension: this shows that complete wetting is enhanced by negative line tension, provided that it would already happen in the absence of line tension.

IV. CONCLUSIONS

We performed a stability analysis of the equilibria of a sessile droplet lying upon a rigid, flat, and homogeneous substrate in the presence of line tension. As expected, we obtained different outcomes depending on the sign of the line tension. While our analysis strengthens Widom's results [7] when the line tension is positive, qualitatively new results occur when the line tension is negative. In accordance with the mathematical properties of the free-energy functional, no equilibrium can definitely be stable for negative line tensions. Although mathematically unquestionable, this conclusion could be misleading since the modes inducing instability may be effective at a length scale incompatible with the model. Enforcing a selection of the class of admissible perturbations makes negative values of the line tension compatible with the existence of stable equilibria, at least if the absolute value of the line tension is not too high, as shown in [11].

We made these qualitative arguments precise by introducing the notion of residual stability, quantitatively measured by an integer m_{rs}. The higher is m_{rs}, the more are the stable modes of a sessile droplet with negative line tension. A typical length ℓ_{rs} was also associated with m_{rs}, which measures the shortest length scale at which the mode with index m_{rs} deforms the unperturbed equilibrium configuration of the droplet. According to our criterion, the droplet is stable whenever ℓ_{rs} is smaller than a microscopic length ℓ_{mic} characteristic of the fluid and unstable otherwise. This criterion was indeed applied to the experimental data published in [14]: for one droplet we checked that $\ell_{\mathrm{rs}} \lesssim \ell_{\mathrm{mic}}$, and so we concluded that the negative line tension measured there is far more reliable than the ideal value estimated in [7], for which $\ell_{\mathrm{rs}} \gtrsim \ell_{\mathrm{mic}}$.

The unstable modes singled out by our analysis are *static*, as they are virtual perturbations. The way in which these modes drive the system out of equilibrium and their role in dynamics are questions left untouched by our treatment, as they would require a *dynamic* instability analysis. However,

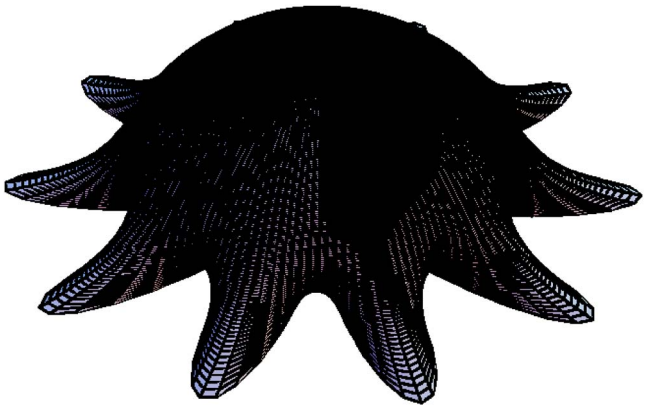

FIG. 10. (Color online) A spherical cap perturbed by a marginal mode with $m_{\mathrm{rs}}=10$. The perturbed contact line exhibits a periodic structure with ten fingers.

as shown in Appendix G, the mean curvature of the droplet's free surface perturbed by marginal modes is still constant up to first order in the perturbation parameter ϵ in Eq. (9). Hence, to the same degree of approximation, the perturbed shape represents an admissible equilibrium shape. This suggests that marginal modes dictate the shape of the droplet in the early stages of its evolution away from an unstable equilibrium configuration. For illustrative purposes only, in Fig. 10 we show a spherical cap perturbed by a marginal mode with $m_{\mathrm{rs}}=10$.

This paper calls for an extension to the case where the effects of line tension are coupled with the curvature of the substrate. This study is indeed currently pursued and will be published elsewhere [19].

ACKNOWLEDGMENTS

We gratefully acknowledge an inspiring discussion with Dr. R. Lipowsky on the need of properly defining the characteristic length ℓ_{rs} and of confronting it with ℓ_{mic}. Financial support for our research was provided by the Italian MIUR under PRIN Grant No. 2004024508.

APPENDIX A: MODES WITH $\nu=0$

As noted in Sec. III, the case $\nu=0$ is rather peculiar since the constant c in Eq. (25) remains undetermined. Here, we determine directly solutions to Eq. (17) that are rotationally invariant—that is, with $m=0$. For $\nu=0$ the scaled multiplier $\mu=-2$. A solution $u=u(\vartheta)$ of Eq. (17) must satisfy

$$u'' + \cot\vartheta u' = \varrho, \tag{A1}$$

where a prime stands for differentiation with respect to ϑ, and ϱ has been rescaled to R^2. We look for solutions that are bounded at $\vartheta=0$. Equation (A1), can be recast as

$$(u' \sin\vartheta)' = -(\varrho\cos\vartheta)',$$

which, once integrated, yields

$$u' = \frac{c_1 - \varrho\cos\vartheta}{\sin\vartheta},$$

where c_1 is an integration constant. Integrating this equation again, we arrive at

$$u(\vartheta) = c_1 \ln\tan\frac{\vartheta}{2} - \varrho\ln\sin\vartheta + c_2.$$

This function is bounded at $\vartheta=0$, provided that $c_1=\varrho$; after some rearrangements, we then arrive at

$$u(\vartheta) = c_2 - \varrho\ln(1+\cos\vartheta).$$

By imposing the incompressibility constraint (26),

$$\int_0^{\vartheta_c} u(\vartheta)\sin\vartheta d\vartheta = 0,$$

we finally obtain

$$c_2 = -\varrho\frac{(1-\cos\vartheta_c) + (1+\cos\vartheta_c)\ln(1+\cos\vartheta_c)}{1-\cos\vartheta_c}$$

and ϱ can be determined by renormalizing the L^2 norm of u on $\mathcal{S}$.

APPENDIX B: STABLE MODES WITH $m=0$

To show that any pair $(\vartheta_c,\varepsilon)$ with negative ε is stable for the mode $m=0$ we prove that it can be attained by the graph of a function $\varepsilon_\nu^0(\vartheta_c)$, for $\nu>1$. To this aim, it is expedient to study the roots in ϑ_c of

$$f(\nu,\vartheta_c) := \nu(1-\cos\vartheta_c)P_\nu(\cos\vartheta_c) + P_{\nu+1}(\cos\vartheta_c) - \cos\vartheta_c P_\nu(\cos\vartheta_c), \tag{B1}$$

where, by Eq. (30b), $\varepsilon_\nu(\vartheta_c)$ could diverge. Let $\bar{\vartheta}_c$ be the smallest, nonvanishing root of Eq. (B1). When ν tends to a natural number n, the function $P_\nu(\cos\vartheta_c)$ tends to the Legendre polynomial $P_n(\cos\vartheta_c)$ in the set $(-1+\eta,1]$, for a positive η, but it diverges logarithmically at $\cos\vartheta_c=-1$: in fact, as a function of a complex variable, $P_\nu(\cdot)$ is analytic only in the complex plane cut along $[-\infty,-1]$. As a consequence, although $f(1,\pi)\neq 0$, the first nontrivial root of $f(\nu,\vartheta_c)$ becomes closer and closer to π, when ν tends to 1—that is,

$$\lim_{\nu\to 1^+}\bar{\vartheta}_c = \pi.$$

On increasing ν, $\bar{\vartheta}_c$ decreases and new roots of Eq. (B1) appear at $\vartheta_c=\pi$, whenever ν approaches a natural number. When $\nu\gg 1$, the asymptotic formula [see Eq. (8.721.3) of [18]]

$$P_\nu(\cos\vartheta_c) = \frac{2}{\sqrt{\pi}}\frac{\Gamma(\nu+1)}{\Gamma\left(\nu+\frac{3}{2}\right)}\frac{\cos\left[\left(\nu+\frac{1}{2}\right)\vartheta_c - \pi/4\right]}{\sqrt{2\sin\vartheta_c}} \times\left[1+O\left(\frac{1}{\nu}\right)\right],$$

where Γ is Euler's function, Stirling's formula [see Eq. (1.4.25) of [16]]

$$\Gamma(x) \approx \sqrt{2\pi}x^{x-(1/2)}e^{-x}$$

and repeated use of the elementary limit

$$\lim_{n\to+\infty}\left(1+\frac{1}{n}\right)^n = e$$

lead us to conclude that

$$f(\nu,\vartheta_c) \approx \sqrt{\frac{2\nu}{\pi}}(1-\cos\vartheta_c)\cos\left[\left(\nu+\frac{1}{2}\right)\vartheta_c - \frac{\pi}{4}\right], \quad \text{for } \nu \gg 1,$$

whence it follows that

$$\lim_{\nu\to+\infty}\bar{\vartheta}_c = 0.$$

Since

$$\lim_{\vartheta_c\to\bar{\vartheta}_c^{\pm}}\varepsilon_\nu(\vartheta_c) = \pm\infty,$$

we conclude that any point of the $(\vartheta_c,\varepsilon)$ plane but $(\pi,0)$ belongs to the graph of some function $\varepsilon_\nu^0(\vartheta_c)$, at least for sufficiently large values of ν.

APPENDIX C: MODES WITH $m=1$

For $m=1$, the following identity holds for all ν [see Eq. (8.733.1) of [18]]

$$(1-x^2)\frac{dP_\nu^1(x)}{dx} = (\nu+1)P_{\nu-1}^1(x) - \nu x P_\nu^1. \tag{C1}$$

Letting $x := \cos\vartheta$, since $dP_\nu^1(\cos\vartheta)/d\vartheta = -\sin\vartheta\,[dP_\nu^1(x)/dx]$, we can recast Eq. (18) as

$$\frac{1}{\sin\vartheta_c}[(1+\nu)P_{\nu-1}^1(\cos\vartheta_c) + (1-\nu)\cos\vartheta_c P_\nu^1(\cos\vartheta_c)] = 0,$$

which is never satisfied when $\nu \neq 1$ and is identically satisfied when $\nu=1$—that is, by Eq. (23)—when $\mu=0$.

APPENDIX D: ASYMPTOTICS OF CONICAL FUNCTIONS

It is easily checked that, when $\lambda>0$, the graphs of $\varepsilon_{-(1/2)+i\lambda}^m(\vartheta_c)$ always lie below that of $\varepsilon_{-1/2}^m(\vartheta_c)$. Here we prove that

$$\lim_{\lambda\to+\infty}\varepsilon_{-(1/2)+i\lambda}^m(\vartheta_c) = -\infty. \tag{D1}$$

When $m=0$, the conical function $P_{-(1/2)+i\lambda}$ has the asymptotic behavior (see p. 202 of [16])

$$P_{-(1/2)+i\lambda}(\cos\vartheta_c) \approx \frac{e^{\lambda\vartheta_c}}{\sqrt{2\pi\lambda\sin\vartheta_c}} \tag{D2}$$

for $\lambda\to+\infty$ and $0<\eta\leqslant\vartheta_c\leqslant\pi-\eta$, with η a positive number. We see from Eq. (30a) that the asymptotic behavior of $\varepsilon_{-(1/2)+i\lambda}^m(\vartheta_c)$ when $\lambda\to+\infty$ is determined by the ratio

$$\frac{1}{P_{-(1/2)+i\lambda}^m}\left.\frac{\partial P_{-(1/2)+i\lambda}^m(\cos\vartheta)}{\partial\vartheta}\right|_{\vartheta_c}.$$

Now, by definition,

$$P_\nu^m(\cos\vartheta_c) := (-1)^m[1-(\cos\vartheta_c)^2]^{m/2}\frac{\partial^m P_\nu(\cos\vartheta_c)}{\partial(\cos\vartheta_c)^m}, \tag{D3}$$

and differentiating both sides in Eq. (D2) with respect to ϑ_c, by Eq. (D3) we show that the leading term in λ of $P_{-(1/2)+i\lambda}^m(\cos\vartheta_c)$ is

$$P_{-(1/2)+i\lambda}^m(\cos\vartheta_c) \approx \frac{\lambda^{(m-1/2)}e^{\lambda\vartheta_c}}{\sqrt{2\pi\sin\vartheta_c}}$$

and, correspondingly,

$$\left.\frac{\partial P_{-(1/2)+i\lambda}^m(\cos\vartheta)}{\partial\vartheta}\right|_{\vartheta_c} \approx \frac{\lambda^{(m+1/2)}e^{\lambda\vartheta_c}}{\sqrt{2\pi\sin\vartheta_c}}.$$

Thus Eq. (D1) follows for all integers m.

APPENDIX E: MODES WITH $m \gg 1$

Here we study the behavior of the marginal curves $\varepsilon_1^m(\vartheta_c)$ as m increases. We first note that, by use of de l'Hôpital's rule in Eq. (31),

$$\varepsilon_1^m(\vartheta_c) := \lim_{\nu\to1}\varepsilon_\nu^m(\vartheta_c) = (\sin\vartheta_c)^3\frac{\left.\frac{\partial P_\nu^m}{\partial\nu}\right|_{\nu=0}}{(m-1)\left.\frac{\partial P_\nu^m}{\partial\nu}\right|_{\nu=1}}, \tag{E1}$$

where we also observed that $\partial P_{\nu-1}^m/\partial\nu|_{\nu=1} = \partial P_\nu^m/\partial\nu|_{\nu=0}$. Strictly speaking, Eq. (E1) holds only away from $\vartheta_c=\pi$, where P_ν^m diverges. This divergence, however, does not concern us here, since we only consider partial wetting. Since [see Eqs. (8.762.1) and (8.762.3) of [18]]

$$\left.\frac{\partial P_\nu(\cos\vartheta_c)}{\partial\nu}\right|_{\nu=0} = 2\ln\cos\frac{\vartheta_c}{2}$$

and

$$\left.\frac{\partial P_\nu^{-1}(\cos\vartheta_c)}{\partial\nu}\right|_{\nu=1} = -\frac{1}{2}\tan\frac{\vartheta_c}{2}\left(\sin\frac{\vartheta_c}{2}\right)^2 + \sin\vartheta_c\ln\cos\frac{\vartheta_c}{2},$$

by use of the identity [see Eq. (8.752.2) of [18]]

$$P_\nu^{-1}(\cos\vartheta_c) = -\frac{\Gamma(\nu)}{\Gamma(\nu+2)}P_\nu^1 = \frac{P_\nu^1}{\nu(\nu+1)},$$

we readily obtain that

$$\left.\frac{\partial P_\nu^1(\cos\vartheta_c)}{\partial\nu}\right|_{\nu=1} = \tan\frac{\vartheta_c}{2}\left(\sin\frac{\vartheta_c}{2}\right)^2 - 2\sin\vartheta_c \ln\cos\frac{\vartheta_c}{2}.$$

Thus, by recalling definition (D3) and interchanging in the order of differentiation, we see from Eq. (E1) that $\varepsilon_1^m(\vartheta_c)$ behaves like $1/m$, when $m \gg 1$, and so

$$\lim_{m\to\infty} \varepsilon_1^m(\vartheta_c) = 0.$$

APPENDIX F: UNSTABLE MODES WITH $m=0$

Here, we show that

$$\lim_{\lambda\to+\infty} \varepsilon^0_{-(1/2)+i\lambda}(\vartheta_c) = +\infty \tag{F1}$$

and make use of the continuous dependence of $\varepsilon_\nu^0(\vartheta_c)$ on ν to conclude that the graphs of $\varepsilon^0_{-(1/2)+i\lambda}$ are all above the graph of $\varepsilon^0_{-(1/2)}(\vartheta_c)$. A glance at Eq. (30b) suffices to conclude that the leading term in λ of $\varepsilon^0_{-(1/2)+i\lambda}(\vartheta_c)$ is

$$\varepsilon^0_{-(1/2)+i\lambda}(\vartheta_c) \approx (\sin\vartheta_c)^3 \frac{\left.\frac{\partial P_{-(1/2)+i\lambda}}{\partial\vartheta}\right|_{\vartheta=\vartheta_c}}{c(\vartheta_c,\nu,0) + P_{-(1/2)+i\lambda}}.$$

We use the identity [see Eq. (8.733.1) of [18]]

$$(\nu+1)P_{\nu+1}(x) = (\nu+1)xP_\nu(x) - (1-x^2)\frac{dP_\nu(x)}{dx} \tag{F2}$$

to eliminate $P_{\nu+1}$ from $c(\vartheta_c,\nu,0)$ in Eq. (29) and then resort to the asymptotic expansion (D2), to arrive at Eq. (F1).

APPENDIX G: MEAN CURVATURE OF MARGINAL MODES

When a surface $\mathcal{S}$ is perturbed as in Eq. (9), its total curvature $H=2/R$ becomes [see Eq. (3.3) of [20]]

$$H_\epsilon = H - \epsilon\{\mathrm{tr}(\nabla_s\boldsymbol{\nu})(\nabla_s\boldsymbol{u}) + H\,\mathrm{div}_s\,\boldsymbol{a}\} + o(\epsilon), \tag{G1}$$

where $\boldsymbol{a} := (\nabla_s\boldsymbol{u})^\mathsf{T}\boldsymbol{\nu}$ is a field everywhere tangent to $\mathcal{S}$. By writing

$$\boldsymbol{u} = \boldsymbol{u}_\parallel + u\boldsymbol{\nu}, \tag{G2}$$

where $\boldsymbol{u}_\parallel$ is the tangential part of $\boldsymbol{u}$, and exploiting the identity $(\nabla_s\boldsymbol{\nu})\boldsymbol{\nu}=0$, it is possible to recast $\boldsymbol{a}$ as

$$\boldsymbol{a} = (\nabla_s\boldsymbol{u}_\parallel)^\mathsf{T}\boldsymbol{\nu} + \nabla_s u.$$

It follows from $\boldsymbol{u}_\parallel\cdot\boldsymbol{\nu}=0$ and the symmetry of $\nabla_s\boldsymbol{\nu}$ that $(\nabla_s\boldsymbol{u}_\parallel)^\mathsf{T}\boldsymbol{\nu} = -(\nabla_s\boldsymbol{\nu})\boldsymbol{u}_\parallel$, and so we conclude that

$$\boldsymbol{a} = -(\nabla_s\boldsymbol{u}_\parallel)^\mathsf{T}\boldsymbol{\nu} + \nabla_s u,$$

whence we obtain that

$$\mathrm{tr}\nabla_s\boldsymbol{a} = \mathrm{div}_s\,\boldsymbol{a} = \Delta_s u - \mathrm{div}_s\,(\nabla_s\boldsymbol{u}_\parallel)^\mathsf{T}\boldsymbol{\nu}.$$

By use of the identity

$$\mathrm{div}_s(\mathbf{T}^\mathsf{T}\boldsymbol{v}) = \mathrm{div}_s\,\mathbf{T}\cdot\boldsymbol{v} + \mathbf{T}\cdot\nabla_s\boldsymbol{v},$$

which holds for any smooth tensor and vector fields $\mathbf{T}$ and $\boldsymbol{v}$, and invoking again the symmetry of $\nabla_s\boldsymbol{\nu}$, we arrive at

$$\mathrm{div}_s\,\boldsymbol{a} = \Delta_s u - \boldsymbol{u}_\parallel\cdot\Delta_s\boldsymbol{\nu} - \nabla_s\boldsymbol{\nu}\cdot\boldsymbol{u}_\parallel.$$

By inserting the decomposition (G2) into Eq. (G1) and noting that

$$\mathrm{tr}(\nabla_s\boldsymbol{\nu})(\nabla_s\boldsymbol{u}) = \nabla_s\boldsymbol{\nu}\cdot\nabla_s\boldsymbol{u}_\parallel + u\mathrm{tr}(\nabla_s\boldsymbol{\nu})^2,$$

we obtain

$$\frac{H_\epsilon - H}{\epsilon} = -\Delta_s u - u\mathrm{tr}(\nabla_s\boldsymbol{\nu})^2. \tag{G3}$$

When $\mathcal{S}$ is a spherical cap of radius R,

$$\mathrm{tr}(\nabla_s\boldsymbol{\nu})^2 = \frac{2}{R^2}$$

and Eq. (G3) becomes

$$\frac{H_\epsilon - H}{\epsilon} = -\Delta_s u - \frac{2}{R^2}u.$$

Since marginal modes solve Eq. (17) with $\mu=0$, we conclude that, on marginal modes,

$$\frac{H_\epsilon - H}{\epsilon} = -\varrho.$$

Moreover, by Eq. (25), $\varrho = 2c$ for $\mu=0$, and by Eq. (29) we easily conclude that $H_\epsilon = H$ for all marginal modes with $m \neq 0$, which are precisely those effective when the line tension is negative.

[1] A. Amirfazli and A. W. Neumann, Adv. Colloid Interface Sci. **110**, 121 (2004).

[2] J. W. Gibbs, in *The Collected Papers of J. Willard Gibbs* (Yale University Press, London, 1957), Vol. I, pp. 55–353.

[3] D. J. Steigmann and D. Li, IMA J. Appl. Math. **55**, 1 (1995).

[4] G. Alberti, G. Bouchitté, and P. Seppecher, Arch. Ration. Mech. Anal. **144**, 1 (1998).

[5] R. Lipowsky, P. Lenz, and P. S. Swain, Colloids Surf., A **161**, 3 (2000).

[6] M. Brinkmann, J. Kierfeld, and R. Lipowsky, J. Phys.: Condens. Matter **17**, 2349 (2005).

[7] B. Widom, J. Phys. Chem. **99**, 2803 (1995).

[8] V. G. Baidakov, G. Sh. Boltachev, and G. G. Chernykh, Phys. Rev. E **70**, 011603 (2004).

[9] L. Boruvka and A. W. Neumann, J. Chem. Phys. **66**, 5464 (1977).
[10] R. Rosso and E. G. Virga, J. Phys. A **37**, 3989 (2004); **37**, 8751 (2004).
[11] R. Rosso and E. G. Virga, Phys. Rev. E **70**, 031603 (2004).
[12] M. Brinkmann, J. Kierfeld, and R. Lipowsky, J. Phys. A **37**, 11547 (2004).
[13] K. Sekimoto, R. Oguma, and K. Kawasaki, Adv. Phys. **176**, 359 (1987).
[14] J. Y. Wang, S. Betelu, and B. M. Law, Phys. Rev. E **63**, 031601 (2001).
[15] M. P. do Carmo, *Differential Geometry of Curves and Surfaces* (Prentice-Hall, Englewood-Cliffs, NJ, 1976).
[16] N. N. Lebedev, *Special Functions and their Applications* (Dover, New York, 1972).
[17] See EPAPS Document No. E-PLEEE8-73-101602 for interplay of spherical and conical modes. The document may also be reached via the EPAPS homepage http://www.aip.org/pubservs/epaps.html) or from ftp.aip.org in the directory /epaps/. See the EPAPS homepage for more information.
[18] I. S. Gradshteyn and I. M. Ryzhik, *Table of Integrals, Series, and Products*, 5th ed., edited by A. Jeffrey (Academic Press, San Diego, 1994).
[19] L. Guzzardi and R. Rosso (unpublished).
[20] R. Rosso and E. G. Virga, Proc. R. Soc. London, Ser. A **455**, 4145 (1999).